

***In vivo* characterization of connective tissue remodeling using infrared photoacoustic spectra**

Yuan Qu
Peng Hu
Junhui Shi
Konstantin Maslov
Peinan Zhao
Chiye Li
Jun Ma
Alejandro Garcia-Uribe
Karen Meyers
Emily Diveley
Stephanie Pizzella
Lisa Muench
Nina Punyamurthy
Naomi Goldstein
Oji Onwumere
Mariana Alisio

Kaytelyn Meyenburg
Jennifer Maynard
Kristi Helm
Emma Altieri
Janessia Slaughter
Sabrina Barber
Tracy Burger
Christine Kramer
Jessica Chubiz
Monica Anderson
Ronald McCarthy
Sarah K. England
George A. Macones
Molly J. Stout
Methodius Tuuli
Lihong V. Wang

Yuan Qu, Peng Hu, Junhui Shi, Konstantin Maslov, Peinan Zhao, Chiye Li, Jun Ma, Alejandro Garcia-Uribe, Karen Meyers, Emily Diveley, Stephanie Pizzella, Lisa Muench, Nina Punyamurthy, Naomi Goldstein, Oji Onwumere, Mariana Alisio, Kaytelyn Meyenburg, Jennifer Maynard, Kristi Helm, Emma Altieri, Janessia Slaughter, Sabrina Barber, Tracy Burger, Christine Kramer, Jessica Chubiz, Monica Anderson, Ronald McCarthy, Sarah K. England, George A. Macones, Molly J. Stout, Methodius Tuuli, Lihong V. Wang, "In vivo characterization of connective tissue remodeling using infrared photoacoustic spectra," *J. Biomed. Opt.* **23**(12), 121621 (2018), doi: 10.1117/1.JBO.23.12.121621.

In vivo characterization of connective tissue remodeling using infrared photoacoustic spectra

Yuan Qu,^{a,b,†} Peng Hu,^{a,b,‡} Junhui Shi,^{c,‡} Konstantin Maslov,^c Peinan Zhao,^a Chiye Li,^{a,b} Jun Ma,^b Alejandro Garcia-Urbe,^b Karen Meyers,^a Emily Diveley,^a Stephanie Pizzella,^a Lisa Muench,^a Nina Punyamurthy,^a Naomi Goldstein,^a Oji Onwumere,^a Mariana Alisio,^a Kaytelyn Meyenburg,^a Jennifer Maynard,^a Kristi Helm,^a Emma Altieri,^a Janessia Slaughter,^a Sabrina Barber,^a Tracy Burger,^a Christine Kramer,^a Jessica Chubiz,^a Monica Anderson,^a Ronald McCarthy,^a Sarah K. England,^a George A. Macones,^a Molly J. Stout,^{a,*} Methodius Tuuli,^{a,*,†} and Lihong V. Wang^{c,*}

^aWashington University in St. Louis, March of Dimes Prematurity Research Center, Department of Obstetrics and Gynecology, St. Louis, Missouri, United States

^bWashington University in St. Louis, Department of Biomedical Engineering, St. Louis, Missouri, United States

^cCalifornia Institute of Technology, Caltech Optical Imaging Laboratory, Andrew and Peggy Cherng Department of Medical Engineering and Department of Electrical Engineering, Pasadena, California, United States

Abstract. Premature cervical remodeling is a critical precursor of spontaneous preterm birth, and the remodeling process is characterized by an increase in tissue hydration. Nevertheless, current clinical measurements of cervical remodeling are subjective and detect only late events, such as cervical effacement and dilation. Here, we present a photoacoustic endoscope that can quantify tissue hydration by measuring near-infrared cervical spectra. We quantify the water contents of tissue-mimicking hydrogel phantoms as an analog of cervical connective tissue. Applying this method to pregnant women *in vivo*, we observed an increase in the water content of the cervix throughout pregnancy. The application of this technique in maternal healthcare may advance our understanding of cervical remodeling and provide a sensitive method for predicting preterm birth. © The Authors. Published by SPIE under a Creative Commons Attribution 3.0 Unported License. Distribution or reproduction of this work in whole or in part requires full attribution of the original publication, including its DOI. [DOI: 10.1117/1.JBO.23.12.121621]

Keywords: photoacoustic endoscopy; spectroscopy; cervical examination; tissue hydration.

Paper 180516SSR received Aug. 26, 2018; accepted for publication Nov. 14, 2018; published online Dec. 5, 2018.

1 Introduction

The cervix is a remarkable structure with diametrically opposite functions: it maintains pregnancy by remaining closed and then, in a process called remodeling, softens and dilates to allow delivery of the fetus in labor.¹ Premature cervical remodeling is a critical indicator of impending spontaneous preterm birth. Preterm birth can occur with a remodeled cervix even in the absence of uterine contractions, but uterine contractions do not lead to delivery if the cervix is firm.^{2–4} Nevertheless, current clinical measurements of cervical remodeling are largely obtained by digital examinations, which are subjective and detect only late events, such as cervical effacement and dilation.

The cervix remodels progressively via incompletely understood mechanisms, such as degradation of extracellular matrix proteins and inflammation.^{5,6} These physiological changes are associated with increased tissue hydration.^{7,8} Therefore, a method that can accurately measure cervical hydration during pregnancy has the potential to facilitate our understanding of cervical remodeling and permit more accurate prediction of preterm birth.

Near-infrared spectroscopy is routinely used in industrial applications to quantify the water content in various products,

because this method is nondestructive and does not require sample preparation.^{9,10} As an embodiment of near-infrared spectroscopy, spectroscopic photoacoustic tomography has been demonstrated in the quantification of various biochemical constituents.^{11–14} However, the previous applications used tabletop systems, which precluded *in vivo* use in the gastrointestinal tract and urogenital tract. Photoacoustic endoscopy (PAE) incorporates an acoustic detector, optical components, and electronic components in a millimeter-diameter-scale probe to image tissue that is inaccessible by tabletop systems.^{15–20}

For the quantification of the water content of the cervix in a pregnant woman, the combination of PAE and near-infrared spectroscopy provides an optimal solution. However, the task is nontrivial, because PAE needs an acoustic coupling medium, which generally contains water as well. The photoacoustic signals emitted by the acoustic coupling medium are not easily separable from the signals emitted by the tissue in the near-infrared wavelength range. This challenge so far has precluded the use of near-infrared spectroscopic PAE for the quantification of water content.

Here, we present a near-infrared spectroscopic PAE system that transmits acoustic waves from the tissue to the acoustic detector through an N-BK7 pentaprism. We analyze the measured photoacoustic near-infrared (PANIR) spectra by linear regression. We demonstrate that this method successfully quantifies the water contents of tissue-mimicking phantoms made of gelatin hydrogel. Applying this method to the cervixes of pregnant women, we observe their physiological water contents and a progressive increase throughout gestation.

*Address all correspondence to Molly J. Stout, E-mail: mollystout@wustl.edu; Methodius Tuuli, E-mail: mtuuli@iu.edu; Lihong V. Wang, E-mail: LVW@caltech.edu

†Present address: Indiana University School of Medicine, Department of Obstetrics and Gynecology, Indianapolis, Indiana, United States

‡These authors contributed equally to this work.

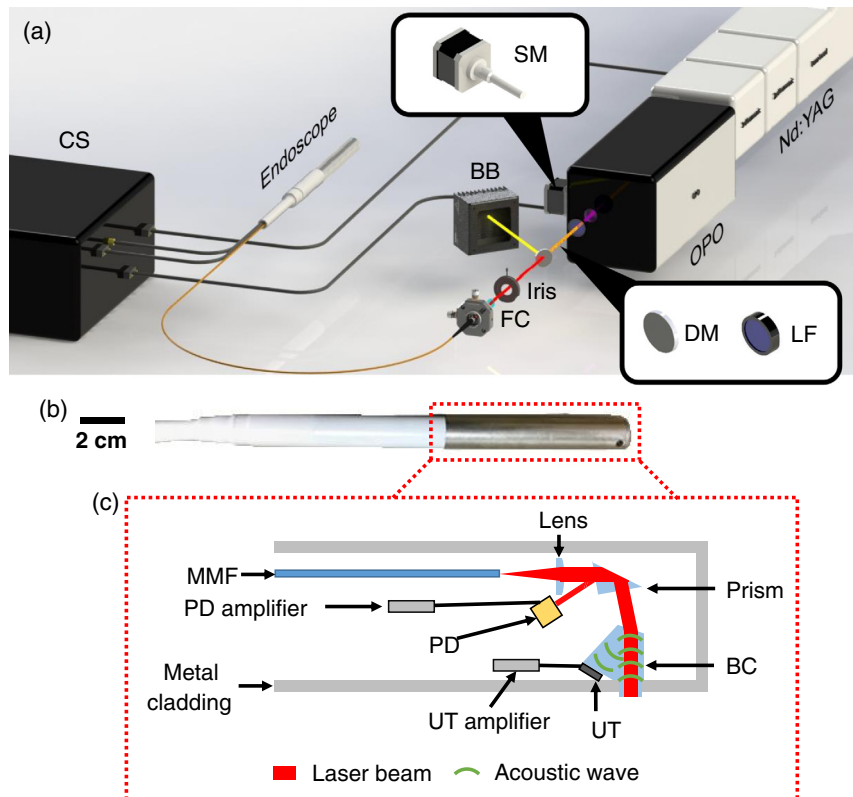


Fig. 1 PANIR system. (a) Setup of the PANIR system. BB, beam block; CS, control system; DM, dichroic mirror; FC, fiber coupler; LF, longpass filter; Nd:YAG, Nd:YAG laser with a frequency tripling module; OPO, optical parametric oscillator; SM, stepper motor. (b) Photograph of a PANIR probe. (c) Schematic of the components in the probe. BC, beam combiner; MMF, multimode fiber; PD, calibrated photodiode; UT, ultrasonic transducer.

2 Methods

2.1 System Setup

We developed the PANIR system shown in Fig. 1(a). The system is controlled by a custom-designed program written in LabVIEW (National Instruments). A frequency-tripled Nd:YAG laser (Quantel, Q-smart 450), operating at 355-nm wavelength with a 20-Hz pulse repetition rate, pumps an optical parametric oscillator (GWU-Lasertechnik, basiScan). A stepper motor moves the optical parametric oscillator so that the idler light can be scanned from 1000 to 2000 nm. After passing through the oscillator, the remaining energy of the pump light is absorbed by a longpass filter. The idler light is selected by a dichroic mirror and then coupled into a multimode fiber, which guides the light to the PANIR probe [Fig. 1(b)]. An iris between the dichroic mirror and the fiber coupler controls the delivered optical energy, keeping the optical fluence (mJ/cm^2) on the tissue surface below the American National Standards Institute safe exposure limit.²¹

The internal structure of the PANIR probe, which is 30 cm in the length and 2 cm in the diameter, is shown in Fig. 1(c). The idler light from the multimode fiber is projected onto the tissue surface by a plano-convex lens and a prism and is absorbed by the tissue below the optical-acoustic beam combiner—a custom-designed pentaprism. The backward photoacoustic wave propagates through the beam combiner toward an ultrasonic transducer (2.25-MHz central frequency). The configuration of all these optical and acoustic elements reduces the amount of

light absorbed by the ultrasonic transducer to a negligible level. While the idler light is sweeping over the entire spectral range, the detected photoacoustic signal is always overwhelmed by noise when only air is underneath the beam combiner. The InGaAs photodiode (FD10D, Thorlabs) in the probe continually measures the energy of the idler light to correct for its energy fluctuations in subsequent data processing. Furthermore, every day, we calibrate the PANIR system with graphite to correct for instrument drift.

2.2 Human Studies

Participants were recruited from the patient population attending the Obstetrics and Gynecology Clinic and the Women's Health Center in the Barnes-Jewish Hospital Center for Outpatient Health. Eligibility requirements included an age of 18 or older, the capability of informed consent, and a gestational age of <16 weeks. Exclusions included potential participants who were non-English speaking, unwilling to participate, carrying a twin pregnancy, or showing evidence of major fetal anomalies.

Prior to measuring the cervix, the operator placed a speculum in the vagina, exposing the cervix for PANIR measurements. The PANIR spectrum has a spectral resolution of 5 nm and a scan of one spectrum takes 10 s. All experimental procedures were carried out in accordance with the protocols approved by the Institutional Review Board of Washington University in St. Louis. All participants signed informed consents before inclusion in the study.

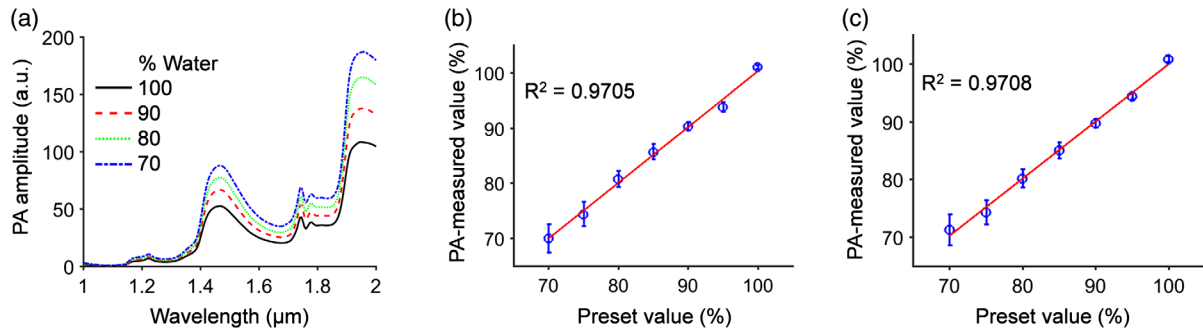


Fig. 2 PANIR spectra quantify the hydration of hydrogel. (a) PANIR spectra measured from hydrogel phantoms made of water and gelatin with different fractions. (b) and (c) Water contents measured at (b) 1460 nm and (c) 1940 nm versus the preset values.

3 Results

3.1 Phantom Experiments

We first quantified the water content in phantoms made of hydrogel because of its similarity to connective tissues.^{22–24} In phantom preparation, a beaker filled with a mixture of gelatin and distilled water was placed on a hot plate and heated to 90°C. A stir bar stirred the mixture at a constant speed. After the gelatin powder was completely dissolved in the mixture, we let the mixture solidify in a Petri dish at room temperature (20°C). When we measured the PANIR spectrum of the phantom, it was kept at 37.5°C to mimic the spectrum of the human cervix, and its weight was measured every hour to track the change of water content due to evaporation. Figure 2(a) shows typical phantoms' PANIR spectra, which move upward as the water content decreases.

To quantify the water content, we fitted a single-wavelength linear regression model based on the empirical calibration because the intercorrelation effect of multiwavelength models led to strong instability.⁹ To minimize the correlation between our measurements and any variation in the environment, we collected PANIR spectra by random sample selection for both

the calibration set and the validation set. The calibration set and the validation set each included 350 PANIR spectra, measured from phantoms whose compositions covered the entire range of water contents in soft human tissues (70% to 100%).²⁵ We tested our method at two wavelengths, 1460 nm, corresponding to the first overtone of O–H stretching, and 1940 nm, corresponding to the second overtone of O–H bending.²⁶ Figures 2(b) and 2(c) show the results and confirm that the measurements of water content agree with the preset values. As the water content in the hydrogel decreased, the standard deviation of our measurements increased, because the gel network became more heterogeneous,²⁷ causing the local water content to fluctuate. At either wavelength, the model provided high and similar prediction accuracies.

3.2 Human Studies

For human cervical tissue, we must consider the effect of scattering, which distorts the PANIR spectrum.²⁸ To understand this influence, we compared our measurements with the results from a Monte Carlo simulation²⁹ that used the optical properties of human tissue.³⁰ Figure 3(a) shows the distortion of the water spectrum by scattering, comparable with the degree found in

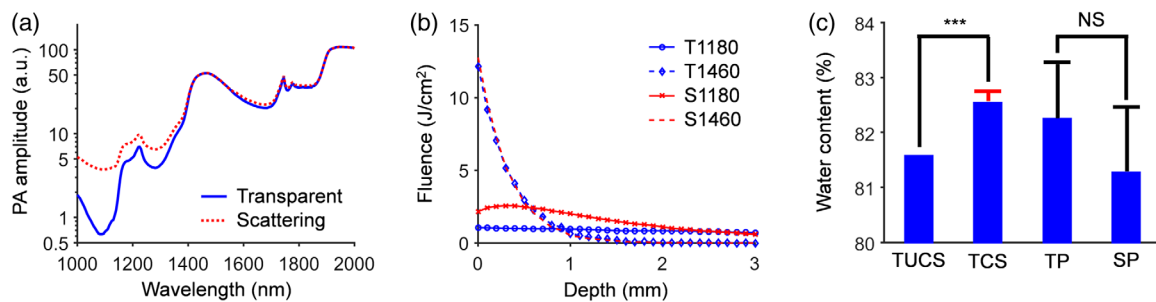


Fig. 3 Effects of scattering simulated by the Monte Carlo method. (a) Effect of scattering on the spectrum. We measured the PANIR spectrum of distilled water (blue) and calculated its spectrum distorted by scattering (red), comparable with the degree found in human skin. (b) Effect of scattering on the distributions of fluence in a medium. The absorption at 1460 nm is so strong that the scattering leads to only a small perturbation of the distribution of fluence. S1180, simulated at 1180 nm in the scattering medium; S1460, simulated at 1460 nm in the scattering medium; T1180, simulated at 1180 nm in the transparent medium; T1460, simulated at 1460 nm in the transparent medium. For illustrative purposes, T1460 and S1460 are divided by a factor of two. (c) Quantified water contents for the human tissue and the hydrogel phantoms. The transparent model underestimates the water content of the scattering medium by ~1%. The red error bar and the black error bar, respectively, show the standard deviations contributed by the cross-sectional change of scattering among the tissue samples ($n = 16$)³⁰ and by the heterogeneity of the hydrogel phantoms ($n = 10$). SP, scattering phantom; TCS, tissue corrected for scattering; TP, transparent phantom; TUCS, tissue uncorrected for scattering. ***, $P < 0.001$. NS, nonsignificant.

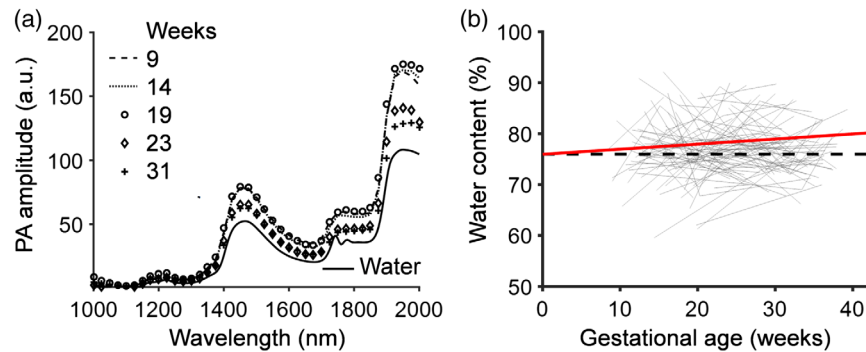


Fig. 4 PANIR spectra quantify cervical remodeling. (a) PANIR spectra measured from the cervix of a pregnant woman at five gestational time points. (b) Longitudinal changes of water contents in the cervixes of pregnant women ($n = 205$), shown as gray lines. The red solid line indicates the fit at the unit level of the generalized linear model to the measured data. The black dashed line represents the level of intercept.

Table 1 Results of the generalized linear model analysis.

	Value	Standard deviation	Degree of freedom	<i>t</i> -value	<i>p</i> -value
Intercept	76.0 (%)	1.1 (%)	204	67.3	0
Slope	0.1 (%/week)	0.1 (%/week)	147	2.2	0.03

human skin. In the wavelength range of 1000 to 1300 nm, where the absorption coefficient ($\mu_a \leq 1 \text{ cm}^{-1}$) was smaller than the reduced scattering coefficient ($\mu'_s \approx 12 \text{ cm}^{-1}$), the PANIR spectrum was raised [Fig. 3(a)] because more photons were absorbed by water than transmitted [Fig. 3(b)]. However, in the neighborhood of 1460 nm, the absorption coefficient ($\mu_a \approx 28 \text{ cm}^{-1}$) was so large that the scattering ($\mu'_s \approx 11 \text{ cm}^{-1}$) caused only a small perturbation in the distribution of fluence [Fig. 3(b)]. As a result, the scattering has little influence on the amplitudes in this neighborhood [Fig. 3(a)]. Without correcting the PANIR spectrum for scattering, the water content of a scattering medium would be underestimated, but only by $\sim 1\%$ [Fig. 3(c)]. This underestimation can be neglected as long as the typical change of water content in a physiological process is much $> 1\%$. In addition, the standard deviation of water contents caused by the cross-sectional change of scattering among the tissue samples was about one order smaller than the underestimation.

Furthermore, we compared the simulation to a phantom experiment in which we made one transparent phantom (hydrogel with 18% gelatin) and one scattering phantom (hydrogel with 1% Intralipid and 17% gelatin). The linear regression model underestimated the water content by $\sim 1\%$ in the scattering phantom, where the reduced scattering coefficient approximated the values used in our simulation. The underestimations in the phantom experiment and in the simulation were consistent. Meanwhile, the heterogeneous gel network resulted in a larger standard deviation of water contents in the measurement, in comparison with the cross-sectional change of scattering in the simulation. These results suggest that scattering will have a minor effect, and the heterogeneity of human tissue will dominate the variation of measured water contents in application.

We validated this method in serial and cross-sectional human studies (Fig. 4), based on the assumption that the hydrogel and the cervical connective tissue were so similar that the regression

model derived from one could be applied to the other.^{22–24}

Figure 4(a) shows the PANIR spectra of a pregnant woman at five gestational time points. The PANIR spectra of the cervix showed little change before 20 weeks' gestation and then dropped to a lower level at the end of the second trimester. We found that the water content increased overall with advancing gestational age [Fig. 4(b)]. The trajectories of water contents, however, were not the same for all patients. We also noticed that the distribution of water contents calculated from the regression model in our study was consistent with the biochemical study.³¹ Furthermore, we carried out a generalized linear model analysis³² to assess the linear association between gestational ages and water contents [Fig. 4(b)]. The data for each patient were grouped and modeled as the random component. The gestational age was the irregularly spaced time variable. The slopes calculated in the analysis (Table 1) indicated that the water content had a significant linear effect with respect to gestational age.

4 Conclusions

We have developed *in vivo* PANIR endoscopy that measures the cervical PANIR spectra of pregnant women. With this new technique, we observed serial and cross-sectional changes in PANIR spectra and cervical hydration in pregnancy. Moreover, the measured cervical hydration was consistent with empirically measured values.³¹ Measurement of PANIR spectra and the cervical hydration levels by our system introduces new possibilities for studying preterm birth. They have the potential to explain how environmental or patient-specific factors increase the risk of preterm birth.^{33–36}

Further research and development of our technology could include direct analysis of PANIR spectra using comprehensive machine learning models, which might reveal other phenomena latent in the spectra beyond human perception.^{37,38} In addition,

the reconstructed PANIR spectrum was a mean spectrum from the area under the beam combiner because the photoacoustic signal was detected by a single-element transducer. As a result, the current lateral spatial resolution is ~ 2.5 mm. Employing a transducer array and photoacoustic computed tomography^{39–42} may enable mapping the PANIR spectrum over the same area with a 100- μm spatial resolution. Other optical methods for quantifying cervical remodeling in pregnant women are being developed.^{43–47} Comparing all optical methods in a large-scale preclinical study would advance our understanding of cervical remodeling from multiple aspects and maximize the prediction accuracy of premature cervical remodeling and preterm birth.

Disclosures

K. Maslov has a financial interest in Microphotoacoustics, Inc. L. V. Wang has a financial interest in Microphotoacoustics, Inc., CalPACT, LLC, and Union Photoacoustic Technologies, Ltd., which, however, did not support this work.

Acknowledgments

We thank Professor James Ballard for closely reading the paper, Li Lin for technical support, and Alicia Brueggemann for help in the study. This project was supported in part by the March of Dimes Prematurity Research Center (3125-17303A) and the National Institutes of Health, Grant Nos. DP1 EB016986 (NIH Director's Pioneer Award) and R01 CA186567 (NIH Director's Transformative Research Award).

References

1. M. Mahendroo, "Cervical remodeling in term and preterm birth: insights from an animal model," *Reproduction* **143**, 429–438 (2012).
2. D. N. Danforth, "The morphology of the human cervix," *Clin. Obstet. Gynecol.* **26**, 7–13 (1983).
3. M. S. Mahendroo et al., "The Parturition defect in steroid 5 α -reductase type 1 knockout mice is due to impaired cervical ripening," *Mol. Endocrinol.* **13**, 981–992 (1999).
4. T. Rechberger, S. R. Abramson, and J. F. Woessner, "Onapristone and prostaglandin E2 induction of delivery in the rat in late pregnancy: a model for the analysis of cervical softening," *Am. J. Obstet. Gynecol.* **175**, 719–723 (1996).
5. B. Timmons, M. Akins, and M. Mahendroo, "Cervical remodeling during pregnancy and parturition," *Trends Endocrinol. Metab.* **21**, 353–361 (2010).
6. J. R. Challis et al., "Inflammation and pregnancy," *Reprod. Sci.* **16**, 206–215 (2009).
7. J. Anderson et al., "Utilization of different aquaporin water channels in the mouse cervix during pregnancy and parturition and in models of preterm and delayed cervical ripening," *Endocrinology* **147**, 130–140 (2006).
8. V. N. A. Breeveld-Dwarkasing et al., "Changes in water content, collagen degradation, collagen content, and concentration in repeated biopsies of the cervix of pregnant cows," *Biol. Reprod.* **69**, 1608–1614 (2003).
9. D. A. Burns and E. W. Ciurczak, *Handbook of Near-Infrared Analysis*, 3rd ed., Taylor & Francis, Hoboken (2008).
10. K. Suehara et al., "Rapid measurement and control of the moisture content of compost using near-infrared spectroscopy," *J. Biosci. Bioeng.* **87**, 769–774 (1999).
11. Z. Xu, C. Li, and L. V. Wang, "Photoacoustic tomography of water in phantoms and tissue," *J. Biomed. Opt.* **15**, 036019 (2010).
12. B. Cox et al., "Quantitative spectroscopic photoacoustic imaging: a review," *J. Biomed. Opt.* **17**, 061202 (2012).
13. T. J. Allen et al., "Spectroscopic photoacoustic imaging of lipid-rich plaques in the human aorta in the 740 to 1400 nm wavelength range," *J. Biomed. Opt.* **17**, 061209 (2012).

14. P. Wang, J. R. Rajian, and J. Cheng, "Spectroscopic imaging of deep tissue through photoacoustic detection of molecular vibration," *J. Phys. Chem. Lett.* **4**, 2177–2185 (2013).
15. J. Yang et al., "Photoacoustic endoscopy," *Opt. Lett.* **34**, 1591–1593 (2009).
16. J. Yang et al., "Simultaneous functional photoacoustic and ultrasonic endoscopy of internal organs in vivo," *Nat. Med.* **18**, 1297–1302 (2012).
17. J. Yang et al., "A 2.5-mm diameter probe for photoacoustic and ultrasonic endoscopy," *Opt. Express* **20**, 23944–23953 (2012).
18. J. Yang et al., "Catheter-based photoacoustic endoscope," *J. Biomed. Opt.* **19**, 066001 (2014).
19. C. Li et al., "Urogenital photoacoustic endoscope," *Opt. Lett.* **39**, 1473–1476 (2014).
20. J. Yang et al., "Optical-resolution photoacoustic endomicroscopy in vivo," *Biomed. Opt. Express* **6**, 918–932 (2015).
21. American National Standards Institute, *American National Standard for the Safe use of Lasers*, American National Standards Institute, Orlando, Florida (2000).
22. M. W. Tibbitt and K. S. Anseth, "Hydrogels as extracellular matrix mimics for 3D cell culture," *Biotechnol. Bioeng.* **103**, 655–663 (2009).
23. N. Gjorevski et al., "Designer matrices for intestinal stem cell and organoid culture," *Nature* **539**, 560–564 (2016).
24. T. Takezawa et al., "Collagen vitrigel: a novel scaffold that can facilitate a three-dimensional culture for reconstructing organoids," *Cell Transplant.* **13**, 463–474 (2004).
25. F. A. Duck, *Physical Properties of Tissue: A Comprehensive Reference Book*, Academic Press, San Diego (1990).
26. R. H. Wilson et al., "Review of short-wave infrared spectroscopy and imaging methods for biological tissue characterization," *J. Biomed. Opt.* **20**, 030901 (2015).
27. R. Tuvikene et al., "Gel-forming structures and stages of red algal galactans of different sulfation levels," *J. Appl. Phycol.* **20**, 527–535 (2008).
28. J. Laufer et al., "In vitro measurements of absolute blood oxygen saturation using pulsed near-infrared photoacoustic spectroscopy: accuracy and resolution," *Phys. Med. Biol.* **50**, 4409–4428 (2005).
29. L. V. Wang, S. L. Jacques, and L. Zheng, "MCML—Monte Carlo modeling of light transport in multi-layered tissues," *Comput. Meth. Programs Biomed.* **47**, 131–146 (1995).
30. T. L. Troy and S. N. Thennadil, "Optical properties of human skin in the near infrared wavelength range of 1000 to 2200 nm," *J. Biomed. Opt.* **6**, 167–176 (2001).
31. K. Myers et al., "Changes in the biochemical constituents and morphologic appearance of the human cervical stroma during pregnancy," *Eur. J. Obstet. Gynecol. Reprod. Biol.* **144S**, S82–S89 (2009).
32. A. Agresti, *Foundations of Linear and Generalized Linear Models*, Wiley, Hoboken, New Jersey (2015).
33. N. Rappoport et al., "A genome-wide association study identifies only two ancestry specific variants associated with spontaneous preterm birth," *Sci. Rep.* **8**, 226 (2018).
34. B. J. Callahan et al., "Replication and refinement of a vaginal microbial signature of preterm birth in two racially distinct cohorts of US women," *Proc. Natl. Acad. Sci. U. S. A.* **114**, 9966–9971 (2017).
35. L. J. Muglia and M. Katz, "The enigma of spontaneous preterm birth," *N. Engl. J. Med.* **362**, 529–535 (2010).
36. K. L. Downes et al., "359: integrating low and high risk cervicovaginal microbiota with antimicrobial peptides may identify those women at greatest risk for spontaneous preterm birth," *Am. J. Obstet. Gynecol.* **216**, S218 (2017).
37. I. Kononenko, "Machine learning for medical diagnosis: history, state of the art and perspective," *Artif. Intell. Med.* **23**, 89–109 (2001).
38. R. O. Duda, P. E. Hart, and D. G. Stork, *Pattern Classification*, 2nd ed., Wiley, New York (2001).
39. L. Li et al., "Label-free photoacoustic tomography of whole mouse brain structures ex vivo," *Neurophotonics* **3**, 035001 (2016).
40. L. Li et al., "Single-impulse panoramic photoacoustic computed tomography of small-animal whole-body dynamics at high spatiotemporal resolution," *Nat. Biomed. Eng.* **1**, 0071 (2017).
41. L. Li et al., "Multiview Hilbert transformation in full-ring transducer array-based photoacoustic computed tomography," *J. Biomed. Opt.* **22**, 076017 (2017).

42. L. Li, L. Lin, and L. V. Wang, "Multiscale photoacoustic tomography," *Opt. Photonics News* **29**(4) 32–39 (2018).
43. C. M. O'Brien et al., "In vivo Raman spectral analysis of impaired cervical remodeling in a mouse model of delayed parturition," *Sci. Rep.* **7**, 6835 (2017).
44. C. M. O'Brien et al., "In vivo Raman spectroscopy for biochemical monitoring of the cervix throughout pregnancy," *Am. J. Obstet. Gynecol.* **218**, 528.e1–528.e18 (2018).
45. M. L. Akins, K. Luby-Phelps, and M. Mahendroo, "Second harmonic generation imaging as a potential tool for staging pregnancy and predicting preterm birth," *J. Biomed. Opt.* **15**, 026020 (2010).
46. Y. Zhang et al., "A compact fiber-optic SHG scanning endomicroscope and its application to visualize cervical remodeling during pregnancy," *Proc. Natl. Acad. Sci. U. S. A.* **109**, 12878–12883 (2012).
47. R. J. Kuon et al., "A novel optical method to assess cervical changes during pregnancy and use to evaluate the effects of progestins on term and preterm labor," *Am. J. Obstet. Gynecol.* **205**, 82.e15–82.e20 (2011).

Biographies of the authors are not available.